Article

Charge Propagation in "Ion Channel Sensors" Based on Protein-Modified Electrodes and Redox Marker Ions

Peter Schn, Tesfaye Hailu Degefa, Simona Asaftei, Wolfdietrich Meyer, and Lorenz Walder

J. Am. Chem. Soc., **2005**, 127 (32), 11486-11496• DOI: 10.1021/ja051574c • Publication Date (Web): 23 July 2005

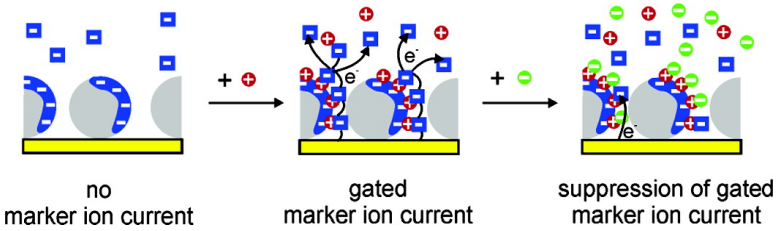

More About This Article

Additional resources and features associated with this article are available within the HTML version:

- Supporting Information
- Links to the 7 articles that cite this article, as of the time of this article download
- Access to high resolution figures
- Links to articles and content related to this article
- Copyright permission to reproduce figures and/or text from this article

View the Full Text HTML

J|A|C|S
ARTICLES
Published on Web 07/23/2005

Charge Propagation in "Ion Channel Sensors" Based on Protein-Modified Electrodes and Redox Marker Ions

Peter Schön,† Tesfaye Hailu Degefa, Simona Asaftei, Wolfdietrich Meyer, and Lorenz Walder*

Contribution from the Institute of Chemistry, University of Osnabrück, Barbarastrasse 7, D-49076, Osnabrück, Germany

Received March 11, 2005; E-mail: LoWalder@uos.de

Abstract: The mechanism of charge propagation in "ion channel sensors" (ICSs) consisting of gold electrodes modified with a layer of charged proteins and highly charged redox-active marker ions in solution was investigated by electrochemical techniques, QCM and AFM. The study is based on seven proteins (concanavalin A, cytochrome *c*, glucose oxidase, lysozyme, thyroglobulin, catalase, aldolase, and EF_1-ATPase) in combination with seven electroactive marker ions ($[Fe(CN)_6]^{3-}$, $[Fe(CN)_6]^{4-}$, $[Ru(NH_3)_6]^{3+}$, mono-, di-, and trimeric viologens), as well as a series of suppressor and enhancer ions leading to the following general statements: (i) electrostatic binding of charged marker ions to the domains of the protein is a prerequisite for an electrochemical current and (ii) charge propagation through the layer consists of electron hopping along surface-confined marker ions into the pores between adsorbed proteins. It is further shown that (iii) marker ions and suppressor ions with identical charge compete for oppositely charged sites on the protein domain, (iv) electrostatically bound multilayers of marker or enhancer ions with alternating charge form on a charged protein domain, and (v) self-exchange and exergonic ET catalysis between adsorbed marker ions and marker ions in solution take place. In addition to fundamental insight into the mechanism of charge propagation, valuable information for the design, optimization, and tailoring of new biosensors based on the ICS concept is demonstrated by the current findings.

Introduction

Over the past 20 years chemists have developed a class of biosensors called **i**on **c**hannel (mimetic) **s**ensors (ICSs) based on highly charged redoxactive marker ions.[1−3] The sensing principle in ICSs consists of the gated flow of charge through an analyte-sensitive barrier membrane, which is supported on an electrode surface. The redox active species are multiply charged ions, so-called marker ions. The sensing membrane is a layer of biological or synthetic material such as peptides,[4,5] proteins,[6−12] DNA,[13−17] or PNA[18−20] attached to the electrode. The signal is the electrochemical current related to the oxidation or reduction of the marker ions at the electrode, i.e., to a heterogeneous electron transfer (ET) underneath the membrane. The gating mechanism is based on molecular recognition of the analyte by the membrane, and this process must influence the conductivity of the membrane. The signal amplification is given by the fact that the analyte has a high affinity with the modifier layer and that a submonolayer coverage of the analyte on the membrane can gate large marker ion currents.

The field of relevant application is impressive, and different mechanistic explanations have been published but usually in a broad context including physical blocking and biological channel proteins.[1] However, the mechanism of the charge propagation through the sensing layer consisting of proteins without intramolecular channels is not yet well understood. Principally, three types of conduction paths must be considered: (1) diffusion of marker ions through interstitial tunnels built from neighboring macromolecules on the gold electrode, (2) redox hopping between surface-confined redox centers describing a

† Present address: Experimental Solid State Physics 2 and Biophysical Chemistry, Institute for Molecules and Materials (IMM), Radboud University Nijmegen, Toernooiveld 1, 6525 ED Nijmegen, The Netherlands.

(1) Umezawa, Y.; Aoki, H. *Anal. Chem.* **2004**, *76*, 320a.
(2) Sugawara, M.; Hirano, A.; Buhlmann, P.; Umezawa, Y. *Bull. Chem. Soc. Jpn.* **2002**, *75*, 187.
(3) Nakano, K. In *Surfactant Science Series*; Hubbard, A. R., Eds.; Dekker: New York, 2001; Vol. ISSS 95, p 512.
(4) Katayama, Y.; Ohuchi, Y.; Nakayama, M.; Maeda, M.; Higashi, H.; Kudo, Y. *Chem. Lett.* **1997**, 883.
(5) Katayama, Y.; Ohuchi, Y.; Higashi, H.; Kudo, Y.; Maeda, M. *Anal. Chem.* **2000**, *72*, 4671.
(6) Kuramitz, H.; Sugawara, K.; Tanaka, S. *Electroanalysis* **2000**, *12*, 1299.
(7) Kuramitz, H.; Sugawara, K.; Nakamura, H.; Tanaka, S. *Chem. Lett.* **1999**, 725.
(8) Gadzekpo, V. P. Y.; Buhlmann, P.; Xiao, K. P.; Aoki, H.; Umezawa, Y. *Anal. Chim. Acta* **2000**, *411*, 163.
(9) Gadzekpo, V. P. Y.; Xiao, K. P.; Aoki, H.; Buhlmann, P.; Umezawa, Y. *Anal. Chem.* **1999**, *71*, 5109.
(10) Murata, M.; Yano, K.; Kuroki, S.; Suzutani, T.; Katayama, Y. *Anal. Sci.* **2003**, *19*, 1569.
(11) Murata, M.; Nakayama, M.; Irie, H.; Yakabe, K.; Fukuma, K.; Katayama, Y.; Maeda, M. *Anal. Sci.* **2001**, *17*, 387.
(12) Murata, M.; Gonda, H.; Yano, K.; Kuroki, S.; Suzutani, T.; Katayama, Y. *Bioorg. Med. Chem. Lett.* **2004**, *14*, 137.
(13) Boon, E. M.; Barton, J. K. *Langmuir* **2003**, *19*, 9255.
(14) Shibata, T. *Anal. Sci.* **2001**, *17 supplement*, i1371.
(15) Maeda, M.; Nakano, K.; Uchida, S.; Takagi, M. *Chem. Lett.* **1994**, 1805.
(16) Maeda, M.; Mitsuhashi, Y.; Nakano, K.; Takagi, M. *Anal. Sci.* **1992**, *8*, 83.
(17) Katayama, Y.; Nakayama, M.; Irie, H.; Nakano, K.; Maeda, M. *Chem. Lett.* **1998**, 1181.
(18) Aoki, H.; Hasegawa, K.; Tohda, K.; Umezawa, Y. *Biosens. Bioelectron.* **2003**, *18*, 261.
(19) Aoki, H.; Umezawa, Y. *Electroanalysis* **2002**, *14*, 1405.
(20) Aoki, H.; Buhlmann, P.; Umezawa, Y. *Electroanalysis* **2000**, *12*, 1272.

10.1021/ja051574c CCC: $30.25

path through the membrane, and (3) electron or hole injection into a conduction band that crosses the membrane. Considering the impact of ICSs and their broad field of application, the elucidation of the mechanism represents not solely an academic problem. It is expected that knowledge of the mechanism of charge propagation (if there exists at all one general mechanism) will help considerably in the design of new ICS sensing membranes and the tailoring of the marker-ion structure.

Recently, we have presented such a general mechanism for SAM-modified electrodes built from long-chain alkanes with charged headgroups on gold electrodes.[21] We have now applied the same technique of investigation to the more complex situation of ICS systems based on protein-modified electrodes. To find general trends, we used a series of seven randomly chosen proteins for the fundamental studies, and more detailed studies were undertaken with one of them, that is, thyroglobulin, showing good stability.

Experimental Section

Chemicals and Reagents. Without further mention, the chemicals were of analytical grade obtained from Aldrich, Merck, or Fluka and used as received. The proteins were: concanavalin A, cytochrome *c* from horse heart, glucose oxidase from *Aspergillus niger* (Sigma) and thyroglobulin from porcine thyroid glands, catalase from *A. niger*, aldolase from rabbit muscle (Fluka). The marker ions, redox-active species and suppressors or gating agents were $K_4[Fe(CN)_6]\cdot 3H_2O$ (Merck), $K_3[Fe(CN)_6]$, 1-ferrocenylethanol, sodium anthraquinone-2-sufonate, disodium 9,10-anthraquinone-2,6-disufonate (Fluka), and $[Ru(NH_3)_6]Cl_3$ (Strem chemicals).

Synthesis. The following compounds and a protein conjugate were prepared earlier or on purpose for this work (the detail of the syntheses are provided in the Supporting Information): (a) new viologen-type marker ions: *N*,*N*′-bis-(2-hydroxylethyl)-4,4′-bipyridinium (**Vio-I**) dibromide, *N*,*N*′-bis-(2-aminoethyl)-4,4′-bipyridinium (**Vio-II**) dibromide, 1,3,5-tris-((*N*-hydroxyethyl-4,4′-bipyridinium)methyl)benzene (**Vio-III**) hexabromide, and carboxybenzyl-3,5-(bis(ethyl-4,4′-bipyridinium)-hexafluorophosphate (**Vio-IV**); (b) a label and its protein conjugate: hydroxymethyl-3,5-(bis(ethyl-4,4′-bipyridinium)-hexafluorophosphate (**P-Vio-IV**), cyctochrome *c*−**Vio-IV** conjugate (**cyt-c-Vio-IV**); and (c) *N*-(2-mercaptoethyl)ferrocene carboxamide (**TF**).

Modification of Electrodes and Substrates. Gold disk electrodes (Metrohm, 6.1204.140, 3 mm diameter) polished to a mirror-finish with a wet Al_2O_3 slurry on a flat pad (Metrohm, 6.2802.000, grain size 0.3 μm), rinsed with distilled water, cleaned for 30 s with fresh piranha solution (2:3 mixture of 30% H_2O_2 and concentrated H_2SO_4). [*Caution: piranha solution must be used with care!*] were used for cyclic and differential pulse voltammetry. The QCM electrodes (plano−plano 5 MHz AT-cut quartz crystals (d = 14 mm, thickness = 330 μm)) with keyhole gold pattern were pretreated as in the case of the disk electrodes except for the polishing step and were used for electrochemical quartz crystal microbalance (EQCM) measurements. For atomic force measurements ultraflat gold surfaces prepared by template stripping according to the procedure of Wagner et al.[22] were used. The freshly cleaned electrodes were incubated in a protein solution for 1 h, and after rinsing with distilled water, they were ready for use. In the case of cytochrome *c*−**Vio-IV**, the solution used for the preparation of the adduct was also used for modifying the gold electrode. When the experiments required filling up the void between the absorbed proteins, the protein-modified electrodes were rinsed with distilled water and then transferred into the thiol solution and incubated for 1 h (for further details see Supporting Information).

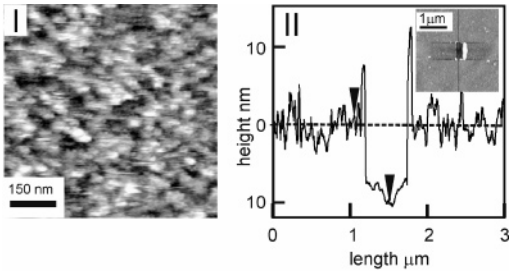

Figure 1. AFM images of thyroglobulin-modified gold surfaces (Tg−Au); (I) 750 × 750 nm (*z*-scale: 8 nm) in liquid tapping mode; (II) height profile over 3000 nm after scratching in contact mode and the corresponding AFM image (inset).

Electrochemical Measurements. All electrochemical measurements were performed in three-electrode systems under Ar, using a potentiostat PGSTAT 20 from AUTOLAB interfaced with a personal computer running under GPES for Windows, version 4.9 (ECO Chemie). In addition to the modified or unmodified gold electrode (working electrode), a Ag/AgCl reference electrode (Methrom, 6.0724.140, separated by a salt bridge containing the electrolyte of the measuring compartment) and a platinum wire as the counter electrode were used. As supporting electrolyte 0.1 M KCl was used, and the pH of the solution was adjusted with 0.1 M NaOH or HCl. Differential pulse voltammetry (DPV) was performed at 25 mV pulse amplitude, 50 ms pulse width, 500 ms pulse period, and 5 mV/s scan rate. Unless otherwise indicated, cyclic voltammetry (CV) was performed at 100 mV/s. All voltammograms are single-scan CVs recorded after 5 s of equilibration at the starting potential. Surface concentrations were calculated from CV using the surface beyond the voltammogram corrected for the capacitive contribution.

EQCM Measurements. The cell used for EQCM was a modified three-electrode construction, described in the literature, allowing the use of flowing (3 mL/min) or quiet electrolyte solutions.[23] The oscillator circuit was from the commercial EQCM cell type 230 (Institute of Physical Chemistry, Warszawa, Poland). Otherwise the same equipment was used as for electrochemistry. For further details see the Supporting Information.

Atomic Force Microscopy. For AFM measurements a Nanoscope IV multimode instrument (Veeco/digital instruments, Santa Barbara, California) equipped with a 12-μm scanner (E scanner) was used in tapping and in contact mode. For further details see the Supporting Information.

Results and Discussion

Formation of the Protein Film. Protein-modified electrodes have been prepared by adsorption of the protein from an aqueous solution of 0.1 mg/mL in 0.1 M KCl onto gold electrodes, as described in the Experimental Section. In the case of thyroglobulin, AFM images indicate a dense coverage of the gold surface (>90%) with the protein mostly in form of a monolayer. Scanning in contact mode in air with high forces on the protein layer removed the adsorbate from the surface without destroying the underlying gold surface. The height profile through the scratched groove shows a vertical distance of ca. 11 nm in good agreement with the calculated molecular diameter of 12 nm of thyroglobulin, indicating monolayer coverage (Figure 1).

Besides closely packed, molecularly resolved proteins, regions of adsorbed unresolved protein clusters are observed in liquid tapping mode. The smallest center-to-center distances of the repetitive globular units is 10−14 nm, again in agreement with

(21) Degefa, T. H.; Schon, P.; Bongard, D.; Walder, L. *J. Electroanal. Chem.* **2004**, *574*, 49.
(22) Wagner, P.; Hegner, M.; Guntherodt, H. J.; Semenza, G. *Langmuir* **1995**, *11*, 3867.
(23) Janshoff, A.; Steinem, C.; Sieber, M.; Galla, H. J. *Eur. Biophys. J Biophys.* **1996**, *25*, 105.

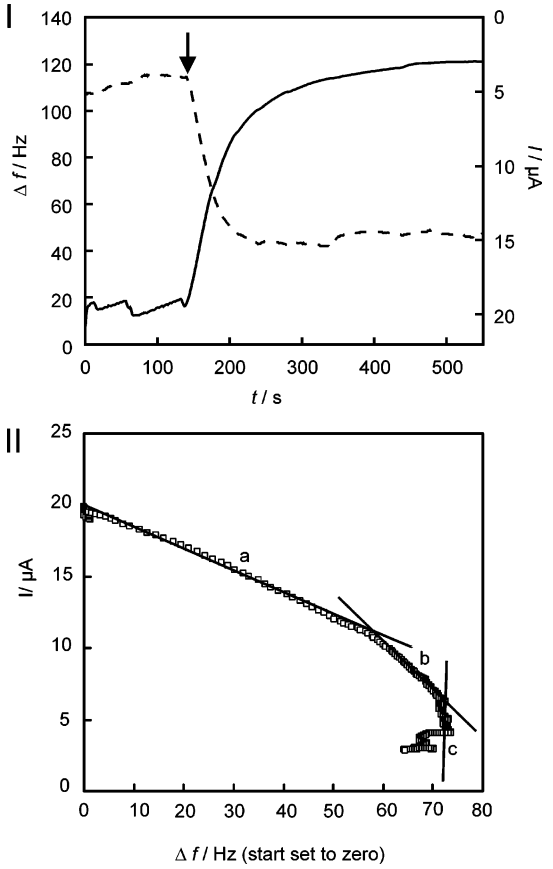

Figure 2. (I) Frequency change (broken line) and anodic current (solid line) of the EQCM vs time. Arrow: addition of Tg (0.1 mg/mL) to the flowing aqueous electrolyte (3 mL/min, KCl (0.1 M, pH = 7) + $[Fe(CN)_6]^{4-}$ (1 mM)); $E = 0.2$ V (vs Ag/AgCl). (II) Current vs frequency change, regions a, b, and c with slopes 15, 650, and ∞nA/Hz, respectively.

the model for the protein size, and with an early electron microscopy study.[24]

The EQCM experiments brought further insight into the process of nonspecific protein adsorption (Figure 2). Upon filling the flow-through cell with a thyroglobulin solution (0.1 mg/mL in 0.1 M KCl, pH 7), the frequency decreased exponentially to reach a constant value of 70 ± 5 Hz below the starting value after ca. 120 s. This corresponds to a change in a mass density ($\Delta\Gamma$) of 1.24 μg cm^{-2}. The value is comparable to the theoretical value ($\Delta\Gamma = 0.9$ μg cm^{-2}) calculated from a simple model, that is based on hexagonal densely packed spheres of 11.9 nm diameter (see Supporting Information). The difference between the theoretical and the experimental value, i.e., 0.34 μg cm^{-2} or 27% could be related to water entrapped within the interstitial void[6] between the surface-confined proteins. Such solvent has been shown to behave as "frozen" with respect to its contribution to the frequency.[25] Hydrodynamically coupled water on the solution side of the layer may be responsible for a further frequency offset.[26]

We used electroactive $[Fe(CN)_6]^{4-}$ as an electroactive ingredient in the circulating electrolyte of the EQCM experiment. Thus, it was possible to monitor simultaneously with the frequency drop the current related to the oxidation of $[Fe(CN)_6]^{4-}$ (marker ion currents were earlier used to monitor protein film formation,[27] but the EQCM arrangement had not been used previously). For this purpose the quartz was potentiostated in the diffusion-limited regime (at $E = 0.2$ V vs Ag|AgCl). As the electrolyte was circulating during the whole experiment, a constant diffusion-layer thickness was established at the electrode surface, and the change in bulk concentration of $[Fe(CN)_6]^{4-}$ was negligible. As a first approximation, the current decrease can be interpreted as the isolating effect of the adsorbing protein. Both observables (frequency and current) seem to be closely related when both are plotted against time (Figure 2, I). A more detailed picture is produced from a plot of current vs frequency values (at identical measuring times, Figure 2, II). Three regions, a, b, and c, can be distinguished. In region a, corresponding to the first 50 s after protein addition and comprising ca. 85% of the whole mass growth, the current and the frequency are linearly correlated with a slope of 15 nA/Hz. Probably, the a region represents the diffusion-limited growth of the protein coating at free electrode sites. In the b region (50−250 s), a linear correlation with a much steeper slope of 650 nA/Hz is observed, i.e. increasing electrochemical isolation with only a small weight increase. Finally, in region c, corresponding to the longest period (between 250 and 550 s), a "vertical line" overlaid by substantial QCM drift and noise is observed. Probably, in region b and c replacement of tight QCM-coupled water in the pores between the proteins and/or conformational changes of the proteins takes place, i.e., processes that help to close the residual electrochemical leakages with little or no change of the quartz frequency.

pH-Controlled Gating of the Redox Currents. When the thyroglobulin-modified electrode is exposed to a solution of the negatively charged marker ion $[Fe(CN)_6]^{4-}$, the differential pulse voltammetric response depends crucially on the pH of the solution. If the pH is reduced from 10 to 3, i.e., upon changing the surface charge of the thyroglobulin layer from mainly negatively charged to positively charged domains, the current rises from residual values to diffusion-controlled values (filled stars in Figure 3,I). On the other hand, if the protein-modified electrode is exposed to a solution containing the positively charged marker ion $[Ru(NH_3)_6]^{3+}$, the current response is switched from low to high values, if the pH is varied from 3 to 10 as the surface charge changes from positive to negative (open triangles in Figure 3, I). The neutral marker ion ferrocenylethanol does not show a pH dependence over the entire pH (filled pentagons in Figure 3, I), as is the case for the charged marker ions on a bare gold electrode (shaded region in Figure 3, I), except for $[Fe(CN)_6]^{4-}$ which drops by less than 20% at pH values larger than 8. These observations are in agreement with reports on gold electrodes modified with alkane thiols with a pH-controllable charge at the headgroup.[26,28−30] For protein-modified electrodes, the pH-dependent gating of redox currents has been observed (or has been tacitly assumed to be present), but no detailed study is available.[27,31]

(24) Berg, G.; Dahlgren, K. E. *Biochim. Biophys. Acta* **1974**, *359*, 1.
(25) Ijiro, K.; Sunami, H.; Arai, K.; Matsumoto, J.; Karthaus, O.; Kraemer, S.; Mittler, S.; Nishi, N.; Juskowiak, B.; Takenaka, S.; Knoll, W.; Shimomura, M. *Colloid Surf., A* **2002**, *198*, 677.
(26) Sugihara, K.; Teranishi, T.; Shimazu, K.; Uosaki, K. *Electrochemistry* **1999**, *67*, 1172.
(27) Moulton, S. E.; Barisci, J. N.; Bath, A.; Stella, R.; Wallace, G. G. *J. Colloid Interface Sci.* **2003**, *261*, 312.
(28) Wang, Y.; Kaifer, A. E. *J. Phys. Chem.* **1998**, *102*, 9922.
(29) Zhao, J. W.; Luo, L. Q.; Yang, X. R.; Wang, E. K.; Dong, S. J. *Electroanalysis* **1999**, *11*, 1108.
(30) Kim, K.; Kwak, J. *J. Electroanal. Chem.* **2001**, *512*, 83.
(31) Kuramitz, H.; Matsuda, M.; Sugawara, K.; Tanaka, S. *Electroanalysis* **2003**, *15*, 225.

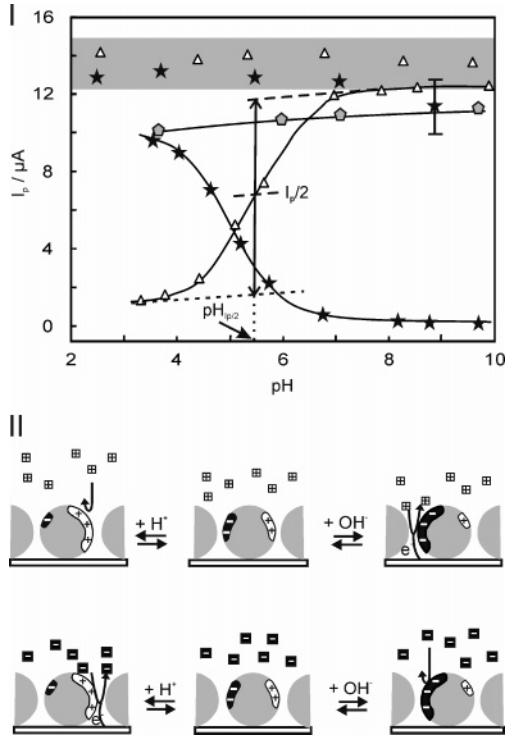

Figure 3. (I) pH dependence of differential pulse voltammetry (DPV) currents of 1 mM $[Fe(CN)_6]^{4-}$ (filled stars), $[Ru(NH_3)_6]^{3+}$ (open triangles) and ferrocenylethanol (filled pentagons) at Tg−Au and at bare Au electrodes (shaded region). (II) Simple model for the heterogeneous ET of highly negatively (black squares) or positively (white squares) charged electroactive marker ions at Tg−Au with positively and negatively charged domains.

The common[1,2,32] model for the pH-induced gating of charged marker ions at protein-modified electrodes is shown in Figure 3, II. It is based purely on the repulsion of marker ions from equally charged protein domains and the concomitant breakdown of the heterogeneous ET. The fact that the neutral ferrocene passes through the layer, whereas the marker ions with the same charge sign as the protein are repelled, points to charge carrying protein side chains with ion exchange properties which extend into the pores.

From the model one may expect a correlation of the titration curves shown in Figure 3, I, and the isoelectrical point (pI) of the protein. Hence, at a pH > pI, with the protein exhibiting a negative net charge, one would expect the negatively charged marker ion to be repelled and the positively charged one to pass and vice versa for pH < pI. To quantify the effectiveness of suppression of the current, we have introduced the values $I_p/2$ and $pH_{I_p/2}$, i.e., half the maximum current on the titration curve and the corresponding pH (see Figure 3, I). The $I_p/2$ and $pH_{I_p/2}$ values for $[Fe(CN)_6]^{4-}$ and $[Ru(NH_3)_6]^{3+}$ are 4.6 and 3.4, respectively, and compare well with the pI value of 4.5 of thyroglobulin **(**see Table 1). However, this correlation does not apply in general.[6] We have measured the "titration curves" of different proteins absorbed on gold electrodes using the marker ions $[Fe(CN)_6]^{4-}$and $[Ru(NH_3)_6]^{3+}$, and we have extracted the $I_p/2$ and $pH_{I_p/2}$ values. The results are listed in the Table 1, together with pI and further information related to the shape of the titration curve. A gap up to 3 pH units is observed between the $pH_{I_p/2}$ values for the anionic and the cationic marker ions,

Table 1. Marker Ion Titration Curve at Protein-Modified Electrodes[a]

		$[Fe(CN)_6]^{4-}$	$[Ru(NH_3)_6]^{3+}$	$[Fe(CN)_6]^{4-}$		$[Ru(NH_3)_6]^{3+}$	
protein	pI	$pH_{Ip/2}$	$pH_{Ip/2}$	I_{max}	I_{min}	I_{max}	I_{min}
cytochrome C	9.3	6	3	13.4	0.7	12.3	3.6
concanavalin A	5	5.1	3.3	9.6	0	9.8	1.4
aldolase	6.1	4.8	4.2	10.7	0	8.8	1.0
glucose oxidase	4.2	6.5	3.3	13.8	2.7	12.5	5.9
catalase	5.4	5.1	4	13.3	0	12.1	1.0
EF_1-ATPase	5	5.4	4.2	10.0	1.0	12.0	1.0
thyroglobulin	4.5	4.6	3.4	9.1	0.1	10.7	1.4

[a] pI: isoelectric point from literature.[33,34] $pH_{I_p/2}$: half current, I_{max} and I_{min}: maximum and minimum current from the titration curve using the indicated marker ion.

and some of the reported pI values are located outside this pH range. Different reasons may account for these findings. First, $pH_{I_p/2}$ values are related to the amount of excess charge that is necessary to repel the marker ion so that the current drops to one-half of its original value, whereas the pI value is defined as the pH at which the sum of negative and positive charge on the protein is zero. The gating efficiencies, i.e., $pH_{I_p/2}$ values, may dependent on the position of the responsible domains on the adsorbed protein, whereas no topological restrictions are expected for the pI value. Moreover, the isoelectric point of an adsorbed protein may differ substantially from the one measured in solution.

As we will show in the following sections, the model shown in Figure 3, II is not adequate to successfully explain the charge transfer of marker ions through protein layers, particularly when the marker ion and the protein layer possess opposite charges.

Influence of the Charge of the Marker Ion on the Gated Current. Having established the role of the charge of the protein, the role of the charge on the marker ion in solution is addressed. For this purpose, we have used three types of marker ions: (i) the well-known transition metal redox marker ions, $[Ru(NH_3)_6]^{3+/2+}$ and $[Fe(CN)_6]^{4-/3-}$; (ii) the commercially available di- and monosulfonated anthraquinoues, 2,9-$AQDS^{2-}$ and 2-AQS^{1-}, respectively; and (iii) three cationic viologens, **[Vio-I]**$^{2+/1+}$, **[Vio-II]**$^{4+/3+}$, and **[Vio-III]**$^{6+/3+}$ designed and prepared for this study because of their different charges (Figure 4 and Supporting Information). During the electrochemical measurement the charge of the redox marker is generally changing, and this influences the electrostatic interaction energy between the protein and the marker ion. It is therefore appropriate to use the average charge, reflecting both redox states of the marker ion. Notably, the anthraquinones both show two couples with a pH-dependent interconversion.[35−37] Thus, we have analyzed the sum of the two peaks, and we have assigned an overall charge of −2 and −1 for 2,9-$AQDS^{2-}$ and 2-AQS^{1-}, respectively. The **[Vio-II]**$^{4+/3+}$ has two basic amine groups, both of them protonated in the pH region of interest (see Supporting Information), and **[Vio-III]**$^{6+/3+}$ is a trimeric viologen undergoing a three-electron reduction step. Considering the change of charge involved in the redox processes and taking into account the possible protonation steps, the following series

(32) Sugawara, M.; Kojima, K.; Sazawa, H.; Umezawa, Y. *Anal. Chem.* **1987**, *59*, 2842.
(33) Lahiri, J.; Isaacs, L.; Tien, J.; Whitesides, G. M. *Anal. Chem.* **1999**, *71*, 777.
(34) Voet, D.; Voet, J. G. *Biochemie, 1. Auflage*; VCH: Weinheim, 1994.
(35) Jones, T. A.; Perez, G. P.; Johnson, B. J.; Crooks, R. M. *Langmuir* **1995**, *11*, 1318.
(36) He, P. X.; Crooks, R. M.; Faulkner, L. R. *J. Phys. Chem.* **1990**, *94*, 1135.
(37) Sun, L.; Johnson, B.; Wade, T.; Crooks, R. M. *J. Phys. Chem.* **1990**, *94*, 8869.

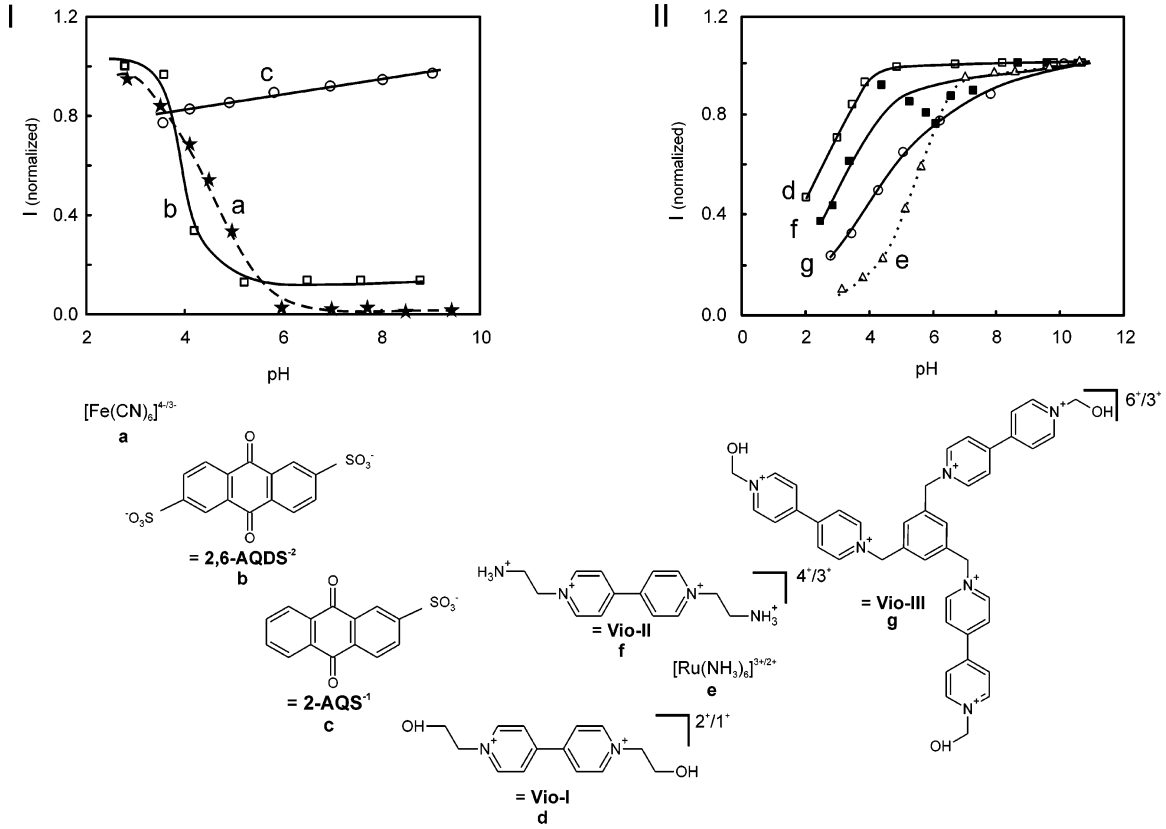

Figure 4. pH-gated DPV currents of marker ions (1 mM) with different charges at Tg−Au; (I) negative marker ions: (a) $[Fe(CN)_6]^{3-/4-}$ (broken line), (b) 2,6-AQDS^{2-} (solid line), (c) 2-AQS^{1-} (solid line); (II) positive marker ions, (d) [Vio-I]$^{2+/+}$ (open squares), (e) $[Ru(NH_3)_6]^{3+/2+}$ (open triangles), (f) [Vio-II]$^{4+/3+}$ (filled squares), (g) [Vio-III]$^{6+/3+}$ (open circles).

of relative charges in our redox marker ions results: $[Fe(CN)_6]^{3.5-}$ < [2,6-AQDS]$^{2-}$ < [2-AQS]$^{-1}$ < [Vio-I]$^{1.5+}$ < $[Ru(NH_3)_6]^{2.5+}$ < [Vio-II]$^{3.5+}$ < [Vio-III]$^{4.5+}$.

In Figure 4, I and II, the normalized titration curves are plotted. In the series [Vio-I]$^{1.5+}$ < [Vio-II]$^{3.5+}$ < [Vio-III]$^{4.5+}$ with structurally closely related species, the influence of the charge on the marker ion becomes evident. The higher the charge on the marker ion, the earlier the suppression is observed when the pH is lowered and positively charged domains are generated on the protein. The same is true for the two anthraquinoues, [2,6-AQDS]$^{2-}$ < [2-AQS]$^{-1}$; the higher the negative charge on the marker, the earlier the suppression is observed when the pH is increased and negatively charged domains are created on the protein. The structurally different $[Ru(NH_3)_6]^{2.5+}$ is blocked better than expected from its charge, indicating that structural reasons are of importance in addition to the charge. With the second and third generation of dendrimers based on **Vio-III**,[38] we found in preliminary work irreversible binding to the protein.

Accumulation of the Marker Ion on the Protein Layer as a Function of pH. The CVs of 4 μM $[Fe(CN)_6]^{4-}$ and 6.6 μM $[Ru(NH_3)_6]^{3+}$ at the thyroglobulin-modified Au (Tg−Au) electrode at pHs 7.5 and 2.5 are shown in Figure 5, I and III, respectively. These pH values have been selected for attractive M^{n+}/P^- and M^{n-}/P^+ interactions (with M^{n+} and M^{n-}: positively and negatively charged marker ion, respectively; and P^- and P^+: negatively and positively charged domains on the protein layer, respectively). Notably, without protein on the surface there is no CV response observable at such low marker ion solution concentrations. The linear dependence of the peak current (I_p) versus scan rate (v) reveals that both marker ions are accumulated at the charged protein[39] (eqs 1 and 5 and Figure 5, II, only shown for the $[Ru(NH_3)_6]^{3+}$ case).

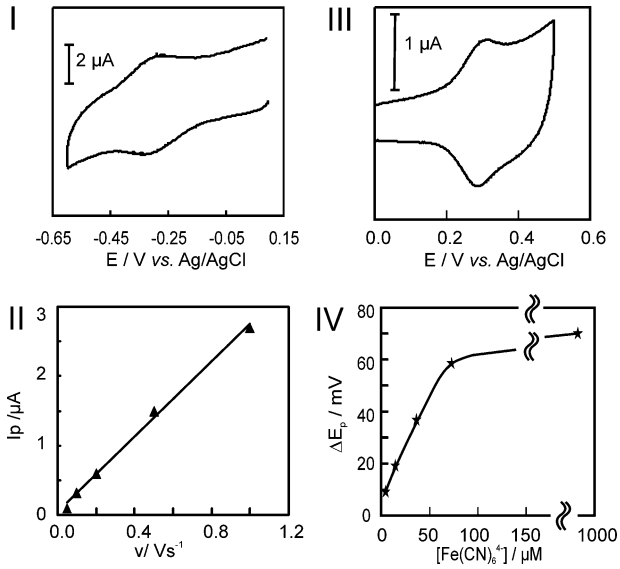

Figure 5. CVs of marker ions at micromolar concentration at Tg−Au; (I−II): marker ion = 6.6 μM $[Ru(NH)_6]^{3+}$ in 10 mM KCl at pH 7.5; (I) CV at v = 0.2 V s^{-1} showing $\Gamma = 100 \times 10^{-12}$ mol cm^{-2}; (II) I_p vs v; (III−IV) marker ion = $[Fe(CN)_6]^{4-}$ in 10 mM KCl at pH 2.5, showing $\Gamma = 23 \times 10^{-12}$ mol cm^{-2}; (III) CV 4 μM $[Fe(CN)_6]^{4-}$ at v = 0.1 V s^{-1}; (IV) ΔE_p as a function of $[Fe(CN)_6]^{4-}$.

(38) Heinen, S.; Walder, L. *Angew. Chem., Int. Ed.* **2000**, *39*, 806.

$$Au/P^- + M^{n+} \rightleftarrows Au/P^- - M^{n+} \quad (1)$$

$$Au/P^+ + M^{n-} \rightleftarrows Au/P^+ - M^{n-} \quad (1a)$$

$$Au/P^- - M^{n+} + e^- \rightleftarrows Au/P^- - M^{(n-1)+} \quad (2)$$

$$Au/P^+ - M^{n-} + e^- \rightleftarrows Au/P^+ - M^{(n+1)-} \quad (2a)$$

In agreement with this observation, the anodic − cathodic peak potential separation (ΔE_p) is 10 mV at 5 μM, it increases to 60 mV (diffusion-controlled value) at 80 μM, and it stays constant into the millimolar range (shown only for the $[Fe(CN)_6]^{4-}$ case, Figure 5, IV). The surface concentrations of the two marker ions are $\Gamma([Ru(NH_3)_6]^{3+}) = 100 \times 10^{-12}$ mol cm^{-2} and $\Gamma([Fe(CN)_6]^{4-}) = 23 \times 10^{-12}$ mol cm^{-2} as calculated from the integration of the CVs in the presence of small concentrations of the marker ions. This surface concentration indicates 54 and 12 marker ions per protein for the ruthenium and for the iron complex, respectively. In agreement, $E°$ of the surface-confined marker ions is different from $E°$ observed in solution because of the preferential stabilization of one of the oxidation states by the counter-charged domain. Electrostatic binding of electroactive ions at charged interfaces is well documented in general,[40] and for SAMs with charged headgroups in particular.[21,41] No evidence from the literature was available thus far for preconcentration of electroactive marker ions at protein-modified electrodes, possibly because most studies were done at marker ion concentrations in the millimolar range, leading to large diffusion-controlled currents which mask the response of surface-confined species.

Suppression and Enhancement of Marker ion Currents: Suppression of Marker Ion Currents (First-Layer Phenomena). A Tg−Au electrode at pH 2.5 in a 1 mM solution of $[Fe(CN)_6]^{4-}$ shows a diffusion-controlled current of the redox-active marker ion (ca. 9 μA, but normalized in Figure 6, I a). If 1,3,5-naphthalene trisulfonate, NTS^{3-}, is added stepwise, the current decreases exponentially and reaches a level of ca. 1.5 μA. On a bare Au electrode, the presence of naphthalene trisulfonate does not influence the electrochemistry of $[Fe(CN)_6]^{4-}$. The explanation is shown in Figure 6, I a, and by the sequence of eqs 3, 2a, and 4, with A^{n-} depicting the suppressor ion.

$$Au/P^+ - M^{n-} + A^{n-} \rightleftarrows Au/P^+ - A^{n-} + M^{n-} \quad (3)$$

$$Au/P^+ - M^{(n+1)-} + M^{n-} \rightleftarrows Au/P^+ - M^{n-} + M^{(n+1)-} \quad (4)$$

Thus, the observed current suppression is explained as follows: In the "pH-opened" situation the domains are covered with marker ions. In this state the redox species shuttle the electrons via lateral electron hopping from the electrode surface to the top of the protein where ET with the same marker ion in solution occurs, eqs 2 and 3 describing a typical electrocatalytic situation. This process seems to be so efficient that currents reach diffusion-controlled levels. When the nonelectroactive ion is added, the surface concentration of the marker ion diminishes and drops below the threshold, which is necessary for effective electron shuttling (eq 4). Besides electron shuttling, there is obviously no important contribution from diffusive pathways of the marker ions to the electrode surface, except the residual current of ca. 1−2 μA in Figure 6, I a).

When the titration curves of micro- and millimolar solutions of $[Fe(CN)_6]^{4-}$ and $[Ru(NH_3)_6]^{3+}$ at the thyroglobulin electrode are normalized and plotted on the same graph, a vertical shift between the two cases is observed (Figure 6, II). Obviously, there is more relative current at a given pH for the millimolar as compared to the micromolar case. In the micromolar range, the titration curve reflects the relative surface concentration of the marker ions, whereas in the millimolar range it reflects a relative current that is gated by the protein surface charge and that can reach diffusion control. Either the marker ion surface concentration as a function of pH grows faster in the millimolar range, and relative catalysis follows the relative surface concentration according to eq 5, or fractional occupancy of the surface sites is sufficient for catalysis to reach diffusion-controlled levels (eqs 3, 4, and 5).

$$Au/P + H^+ + M^{(n+1)-} \rightleftarrows Au/P^+ - H - M^{(n+1)-} \quad (5)$$

Enhancement of Marker Ion Currents (Second-Layer Phenomena). The current response at the thyroglobulin electrode is completely suppressed when a $[Fe(CN)_6]^{4-}$ solution is used as marker ion at pH 8, because of the negatively charged domains on the protein surface. Upon addition of a millimolar amount of Ca^{2+}, the ET barrier drops, and $[Fe(CN)_6]^{4-}$ currents are observed (Figure 7, I). The same happens even in the micromolar range if the viologen **Vio-II** is used instead of Ca^{2+}. The latter ion is electroactive, but in this experiment we only made use of its positive charge and monitored the current only at the $[Fe(CN)_6]^{4-}$ redox potential.

According to the model discussed so far, we expect Ca^{2+} or **Vio-II** to accumulate on the oppositely charged domains of the protein. This leads to charge inversion on the domain. $[Fe(CN)_6]^{4-}$ can then accumulate on the charge-inverted region to yield a double layer on the protein: $P^- - Ca^{2+} - [Fe(CN)_6]^{4-}$ (eqs 6, 7). This supramolecular configuration opens a new ET shuttling path along the protein periphery. The same mechanism has been invoked earlier for SAM-modified electrodes.[21,41]

$$Au/P^- + M^{n-} + Ca^{2+} \rightleftarrows Au/P^- - Ca^{2+} - M^{n-} \quad (6)$$

$$Au/P^- - Ca^{2+} - M^{(n)-} + e^- \rightleftarrows Au/P^- - Ca^{2+} - M^{(n+1)-} \quad (7)$$

$$Au/P^- + M^{n-} + Ca^{2+} \rightleftarrows Au/P^- - Ca^{2+} - M^{n-}(-Ca^{2+} - M^{n-})_n \quad (8)$$

Formation of multiple electrostatically bound layers according to eq 8 cannot be excluded, but this possibility seems not very probable in water. For **Vio-II** a set of equations analogous to eqs 6−8 can be written, but **Vio-II** exhibits a much higher association constant.

Suppression of Charge Propagation through the Outer Layer. As shown above, a second electrostatically bound layer consisting of marker ions can develop on top of a first ionic layer bound to the protein domain. In Figure 6, I b, we demonstrate that it is possible to exchange marker ions in this outer layer by suppressor ions (NTS^{3-}) according to eq 9. Thus, upon addition of naphthalene trisulfonate (NTS^{3-}), the electroactive $[Fe(CN)_6]^{4-}$ ions sitting on top of a protein-confined Ca^{2+} layer are diluted, making the current drop. Such a current suppression related to an exchange in the second ionic layer is

(39) Bard, A. J.; Faulkner, L. R. *Electrochemical Methods; Fundamenatls and Applications*; Wiley: New York, 1980; Chapter 6.
(40) Andrieux, C. P.; Saveant, J. M. In *Molecular Design of Electrode Surfaces*; Murray, R. W., Ed.; Wiley: New York, 1992; Vol. 22, p 207.
(41) Han, X. J.; Wang, E. *Anal. Sci.* **2001**, *17*, 1171.

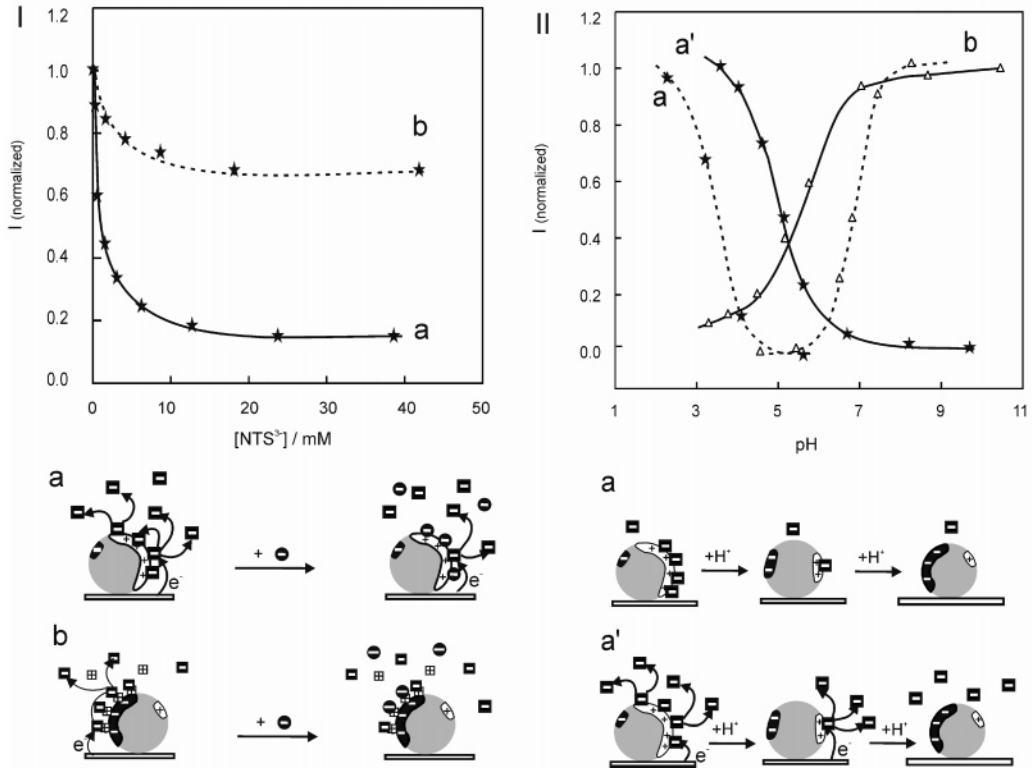

Figure 6. (I) Normalized DPV currents of $[Fe(CN)_6]^{4-}$ (1 mM) at Tg−Au: (a) at pH 2.5 and (b) at pH 7.7 + Vio-II ($c = 0.4$ mM) as function of $[NTS^{3-}]$, and the corresponding models showing first- and second-layer ET; (II) normalized CV and DPV currents at Tg−Au of $[Fe(CN)_6]^{4-}$ at $c = 10.6$ μM, CV (broken line, a) and $c = 1$ mM, DPV (solid line, a′); (b) $[Ru(NH_3)_6]^{3+}$, $c = 6.6$ μM, CV (broken line) and $c = 1$mM, DPV (solid line) as a function of pH, and the ET models for a and a′.

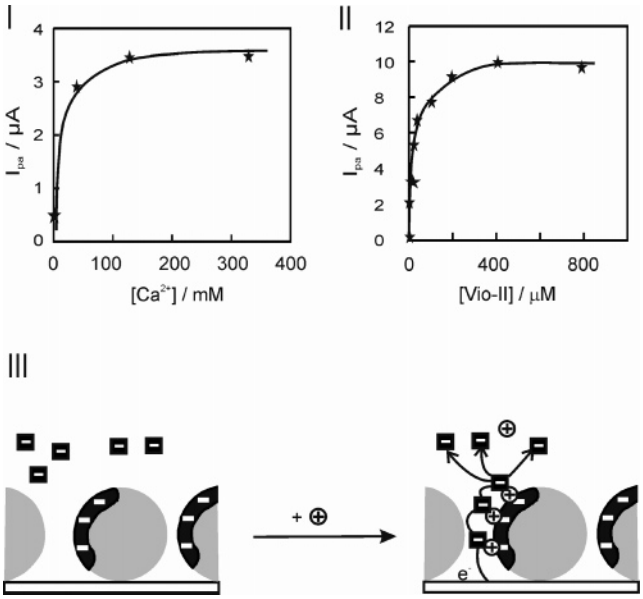

Figure 7. (I, II, III) DPV currents of 1 mM solution of $[Fe(CN)_6]^{4-}$ at Tg−Au at pH 7.8 as function of Ca^{2+} concentration (I), and as a function of $[\mathbf{Vio\text{-}II}]^{4+}$ concentration (II); (III) model for gating of ET induced by inversion of the protein surface charge.

much less effective as compared to the one observed in the first layer for the same suppressor ion NTS^{3-} (see Figure 6, I a). Complicated multilayer structures (eq 8) may be responsible for the reduced suppression efficiency.

$$Au/P^{-}-Ca^{2+}-M^{(n)-} + NTS^{3-} \rightleftarrows Au/P^{-}-Ca^{2+}-NTS^{3-} + M^{(n)-} \quad (9)$$

pH-Independent Surface Charge Controlled by a Covalently Bound Organic Polyion. We have prepared cytochrome *c* (cyt *c*) labeled 2−3 times with the dimeric viologen dendron **Vio-IV** to yield **cyt-c-(Vio-IV)$_n$** with $n = 2-3$ (see Supporting Information). The modified protein exhibits 8−12 additional cationic charges independent of the pH of the solution. It adsorbs on gold as does the unlabeled cyt *c* (Table 1). The viologen labels show up on such electrodes as a wave that is typical for a surface-confined species with a coulometry of $\Gamma = 3.7 \times 10^{-11}$ mol cm^{-2} (Figure 8, I). In a titration experiment, using $[Fe(CN)_6]^{4-}$ as marker ion, the DPV current on the iron redox potential is independent of pH, indicating that the 8−12 persistent charges of the surface-bound viologens dictate the total surface charge of cyt *c*. In contrast to electrodes with native cyt *c*, the $[Fe(CN)_6]^{4-}$ can bind at all pH values to the surface of the labeled cytochrome and can shuttle the electrons at constant rate.

pH-Induced Reversal of the Layer Sequence. A similar independence of the DPV currents from pH as just described for **cyt-c-(Vio-IV)$_n$** is observed for thyroglobulin-modified electrodes (Tg−Au), if a mixture of viologen (**Vio-III**) and $[Fe(CN)_6]^{4-}$ is used as a marker-ion mix (Figure 9). Notably, the concentration was reduced to 0.2 mM to prevent precipitation of the marker ions.

When used solely, each of the marker ions yields "normal" titration curves (see Figure 4). The explanation for the sudden independence from pH is as follows: at high pH with negatively charged domains present, an inner layer of **Vio-III** followed by an outer layer of $[Fe(CN)_6]^{4-}$ builds up (eq 10). Electron transfer to **Vio-III** in solution and from $[Fe(CN)_6]^{4-}$ in solution occurs by ET self-exchange along the corresponding inner and

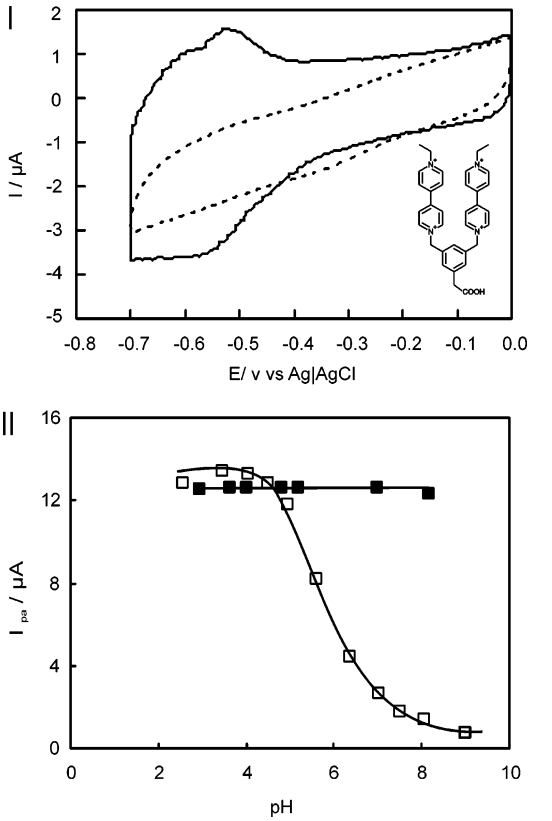

Figure 8. (I) CV of Au electrodes modified with cyt *c* (broken line) and **cyt-c-Vio-IV** conjugate (solid line) exhibiting $\Gamma = 3.7 \times 10^{-11}$ mol cm^{-2}. (Inset) Viologen label for cyt *c*; (II) DPV pH titration of 1 mM $[Fe(CN)_6]^{4-}$ at a cyt *c*-modified Au electrode (open squares) and at a **cyt-c-Vio-IV** conjugate-modified electrode (filled squares).

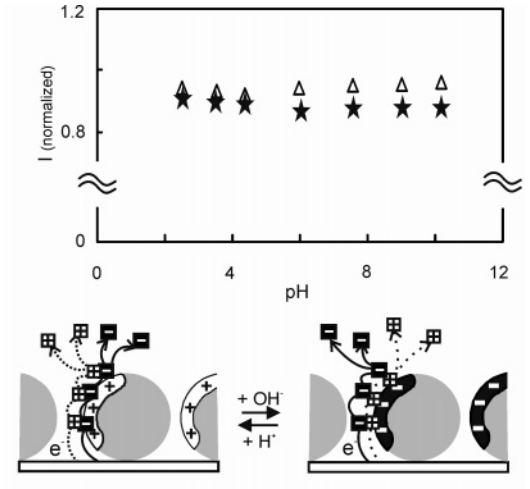

Figure 9. pH dependence of DPV currents of 0.2 mM $[$**Vio-III**$]^{6+/3+}$ and 0.2 mM $[Fe(CN)_6]^{4-}$ at Tg−Au as evaluated on the $[$**Vio-III**$]^{6+/3+}$ and $[Fe(CN)_6]^{4-/3-}$ waves.

outer layers (eqs 11 and 12). When the pH is lowered, the negatively charged domains disappear, and positively charged domains develop on the surface of the protein. The viologen layer breaks up, and the $[Fe(CN)_6]^{4-}$ layer that is sitting on top disintegrates likewise. Simultaneously, a primary $[Fe(CN)_6]^{4-}$ layer develops on the positively charged protein domains, and a viologen layer builds up on top of it (eq 13). Both components of the double layer again catalyze ET independently to or from the corresponding solution redox species (eqs 14 and 15). Thus, an inversion of the sequence of the marker ions in a double ionic layer induced by the charge of the underlying protein domain is postulated.

high pH:

$$Au/P^- + Vio^{++} + Fe(CN)_6^{4-} \rightleftarrows Au/P^- - Vio^{++} - Fe(CN)_6^{4-} \quad (10)$$

$$Au/P^- - Vio^{+} - Fe(CN)_6^{4-} + Vio^{++} + Fe(CN)_6^{4-} \rightleftarrows Au/P^- - Vio^{++} - Fe(CN)_6^{4-} + Vio^{+} + Fe(CN)_6^{4-} \quad (11)$$

$$Au/P^- - Vio^{++} - Fe(CN)_6^{3-} + Vio^{++} + Fe(CN)_6^{4-} \rightleftarrows Au/P^- - Vio^{++} - Fe(CN)_6^{4-} + Vio^{++} + Fe(CN)_6^{3-} \quad (12)$$

low pH:

$$Au/P^+ + Vio^{++} + Fe(CN)_6^{4-} \rightleftarrows Au/P^+ - Fe(CN)_6^{4-} - Vio^{++} \quad (13)$$

$$Au/P^+ - Fe(CN)_6^{4-} - Vio^{+} + Vio^{++} + Fe(CN)_6^{4-} \rightleftarrows Au/P^+ - Fe(CN)_6^{4-} - Vio^{++} + Vio^{+} + Fe(CN)_6^{4-} \quad (14)$$

$$Au/P^+ - Fe(CN)_6^{3-} - Vio^{++} + Vio^{++} + Fe(CN)_6^{4-} \rightleftarrows Au/P^+ - Fe(CN)_6^{4-} - Vio^{++} + Vio^{++} + Fe(CN)_6^{3-} \quad (15)$$

Exergonic ET Catalysis Using Two Oppositely Charged Marker Ions. In the above experiment, using marker **Vio-III** in the oxidized form and $[Fe(CN)_6]^{4-}$ in the reduced form, only ET self-exchange between surface-confined and solution-borne species is possible because of $E°$ (**Vio-III**) $\ll E°$ ($[Fe(CN)_6]^{4-}$). In the following experiment, we have chosen the redox state of the two couples so that exergonic ET between reduced **Vio-I**, generated at the protein surface, and oxidized $[Fe(CN)_6]^{3-}$ in solution is principally possible. **Vio-I** was used at variable concentration ($0-0.4 \times 10^{-3}$ M) and $[Fe(CN)_6]^{3-}$ at constant concentration (1×10^{-3} M). The pH was adjusted for **Vio-I** coordination in the first protein surface layer (pH = 10.3). With no viologen present, the electrode is completely isolated from $[Fe(CN)_6]^{3-}$ in solution because the negative domains repel these marker ions.

Upon addition of 2×10^{-6} M **Vio-I**, a catalytic current peak (ca. 1×10^{-6} A) develops at −0.47 V (potential b in Figure 10), i.e., 0.15 V more positive than $E°'$ of **Vio-I** (−0.64 V), together with a very broad shoulder (c in Figure 10).

low Vio^{2+} concentration:

$$Au/P^- - Vio^{+} + Fe(CN)_6^{3-} \rightleftarrows Au/P^- - Vio^{++} + Fe(CN)_6^{4-} \quad (16)$$

medium Vio^{2+} concentration:

$$Au/P^- - Vio^{+} - Fe(CN)_6^{4-} + Vio^{++} + Fe(CN)_6^{3-} \rightleftarrows Au/P^- - Vio^{++} - Fe(CN)_6^{4-} + Vio^{+} + Fe(CN)_6^{4-} \quad (17)$$

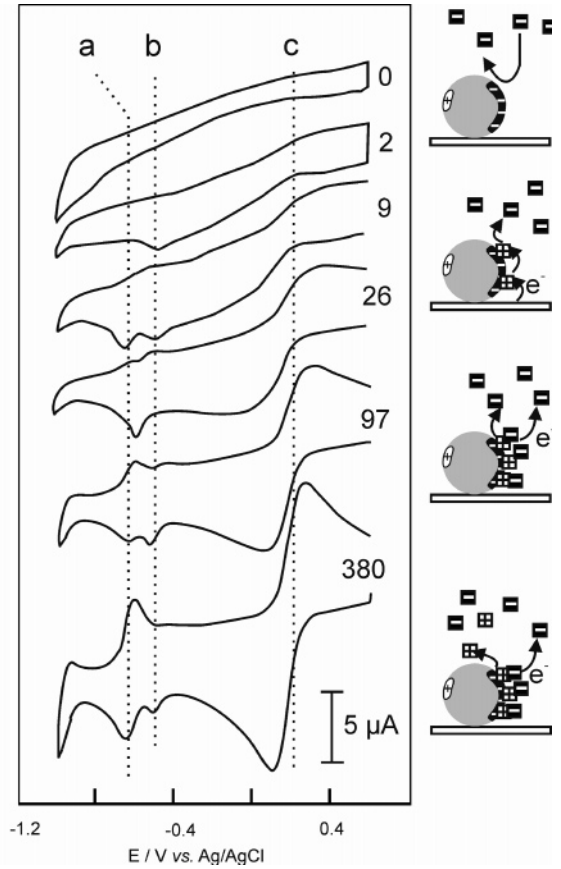

Figure 10. Concurrent exergonic (c) and self-exchange (b) ET catalysis of $[Fe(CN)_6]^{3-}$ reduction at Tg−Au at pH 10.5 as a function of increasing amounts of $[\mathbf{Vio\text{-}I}]^{2+}$; $[Fe(CN)_6]^{3-}$ (c = 1 mM, black squares), $[\mathbf{Vio\text{-}I}]^{2+}$ (c = 0, 2, 9, 26, 97, 380 μM, white squares).

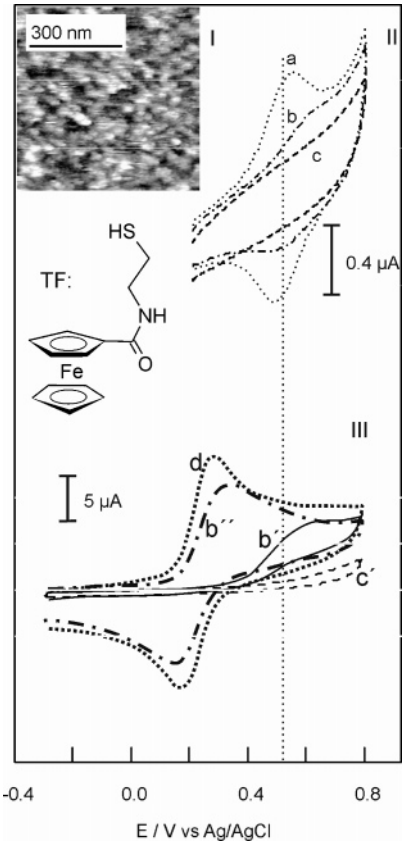

Figure 11. (I) AFM of Tg−Au after **TF** treatment. (II) CV of: (a) **TF**-modified Au electrode showing $\Gamma_{TF} = 9.0 \times 10^{-11}$ mol cm^{-2}; (b) Tg−Au after **TF** treatment showing $\Gamma_{TF} = 1.4 \times 10^{-11}$ mol cm^{-2}; and (c) Tg−Au in 0.1 M $NaClO_4$. (III) CV of 1 mM $[Fe(CN)_6]^{4-}$ in 0.1 M NaClO4 at the Tg−Au at pH 8.5 (c′); Tg−Au after **TF** treatment at pH 8.5 (b′), pH 3 (b″) and blank Au electrode at pH 3 (d). **TF**: thionyl ferrocene.

If the **Vio-I** response would be amplified just by preconcentration (similar to the situation shown in Figure 5 for $[Fe(CN)_6]^{4-}$), it should show a cathodic and anodic response. The presence of only a cathodic response is typical for the electrocatalytic situation described by eq 16. In parallel or slightly delayed with respect to the stepwise increased **Vio-I** concentration, self-exchange ET catalysis of $[Fe(CN)_6]^{3-}$ reduction via hexacyanoferrate sitting on the viologen layer is observed (eq 17). Upon further addition of viologen, the catalytic **Vio-I** peak does not grow significantly, but the rate of self-exchange-catalyzed reduction becomes faster. Upon further successive addition of **Vio-I** the $[Fe(CN)_6]^{3-}$ wave becomes gradually reversible to reach at c(**Vio-I**) = 0.38 mM a diffusion-controlled shape. At this concentration the **Vio-I** wave has also adopted a reversible shape with $E^\circ = -0.62$ V (confirmed also in a similar situation with a SAM-[21] or a DNA-modified electrode[13]).

Testing the Role of the Void between Adsorbed Proteins. Under "pH-opened" condition, there is a large current flow through the protein layer. This must happen via ET self-exchange between surface-confined marker ions, otherwise it would not be possible to suppress such currents with equally charged nonelectroactive ions. As the marker ions can generally not penetrate the protein, the electron-hopping conduction paths along the surface must extend into the pores between adjacent proteins. Thus, the pores, with their inner walls covered with the marker ions, act as "funnels" that guide the current collected on top of the protein to the gold electrode. "Current collection" occurs by ET between diffusing and surface-confined marker ions on top of the protein. The electron can then hop along the domain by self-exchange. Ultimately, it will follow a marker ion-covered finger of the domain that extends deep into the interstitial space. Alternatively, "current collection" could occur by radial diffusion[42] from the semispherical space above a pore toward the redox-conductive pore with a mechanistic change (diffusion/ET self-exchange) at the pore entrance. We studied therefore the importance of the electrode area which is accessible between the adsorbed proteins.

From a model of hexagonal tightly packed disks one expects 9% "free" projected space (see Supporting Information), but from AFM measurements (see Figure 1) the open space related to pores is guessed to be smaller. We used two gold anchoring compounds for this study, i.e., the nonelectroactive long-chain *n*-dodecane thiol and the electroactive *N*-(2-mercaptoethyl) ferrocene carboxamide (**TF**). When the thyroglobulin-coated electrode is further modified with the ferrocene carboxamide, a surface-confined response is observed in pure electrolyte, exhibiting a surface concentration (Γ) of 1.4×10^{-11} mol cm^{-2}. This corresponds to a 15% coverage of the total surface (**TF** shows $\Gamma = 9.0 \times 10^{-11}$ mol cm^{-2} when adsorbed to the same gold electrode but without the protein layer) (Figure 11, II). The thyroglobulin-modified (Tg−Au) electrode with ferrocene carboxamide treatment exhibits electrocatalytic oxidation of $[Fe(CN)_6]^{4-}$ under pH-closed conditions (Figure 11, II b′). The

(42) Choi, S. J.; Park, S. M. *Bull. Korean Chem. Soc.* **2002**, *23*, 699.

catalytic current is ca. 50% of the current for the same electrode under pH-opened conditions (Figure 11, III b″). Using a Tg−Au electrode with *n*-dodecane thiol treatment, no marker ion $[Fe(CN)_6]^{4-}$ current is observed under pH-closed conditions, and at pH-opened conditions, the marker ion current observed is 0.10 of the expected current (Supporting Information).

Preliminary AFM results show that treatment of the protein-modified electrode with the thiols does not damage the protein layer (Figure 11, I, shown for **TF**). Hence, the above results point to the crucial role of the interstitial space between adjacent proteins. The catalytic current observed for $[Fe(CN)_6]^{4-}$ oxidation with no current on the reverse scan points to an ordered sequence of ferrocene carboxamide and $[Fe(CN)_6]^{4-}$, i.e., Au−S−ferrocene−$[Fe(CN)_6]^{4-}$. At a gold electrode modified with the same ferrocene but without protein, no ET catalysis on the ferrocene but direct ET on the $[Fe(CN)_6]^{4-}$ wave is observed (Supporting Information). This points to the important role of the protein in establishing the linear arrangement Au−S−ferrocene−$[Fe(CN)_6]^{4-}$. The extremely reduced current observed for the dodecane thiol-filled interstitial gold spots is presumably due to the interception of the redox conduction path by sequence of reactions shown in eqs 18 and 19.

$$Au/P^+-H\ (aq) + \text{dodecane}-SH \rightleftarrows Au/P(\text{dodecane}-S-Au) + H^+ + H_2O \quad (18)$$

$$Au/P^+-H-[Fe(CN)_6]^{4-}\ (aq) + \text{dodecane-SH} \rightleftarrows Au/P^+-H(\text{dodecane}-S-Au) + [Fe(CN)_6]^{4-} \quad (19)$$

In conclusion, the walls of the pores act as pH-tunable ion exchangers, and the gold surface at the bottom of the pore can be modified with thiols. ET can be suppressed or initiated by the thiols adsorbed on the exposed gold. The large current change related to modifications at the bottom of the pores points to the sensitivity of ICSs in this region.

Implications for ICS Applications. On the basis of the mechanistic criteria established, existing ICS systems can be classified, and the variants with high signal amplification potential are discussed (a−d).

(a) Charged analytes. The marker ion current is either opened (type 1) or suppressed by the analyte interacting with the sensing layer (type 2). Notably, opening a marker ion current is, in principle, more efficient than closing a marker ion current because of the underlying catalysis of ET self-exchange, which amplifies the response.

(a.1.) Opening of a marker ion current was observed in this work using Ca^{2+} and **Vio-II**$^{4+}$ as analytes together with the Tg−Au electrode using $[Fe(CN)_6]^{4-}$ (Figure 7). The same principal approach is known in the literature using $[Fe(CN)_6]^{4-/3-}$ in combination with different analytes, e.g. alkaline earth ions or protonated quinacrine on DNA-modified electrodes,[15,16,43] or alkaline earth ions and lanthanides using an electrode modified with short peptides.[44,45] We assume (and this was stated earlier by some of the authors) that charge inversion and formation of a double ionic layer occurs in all these sensing systems.

(a.2.) Shutting down a marker ion current was observed in this work with $[NTS^{3-}]$ competing with $[Fe(CN)_6]^{4-}$ (Figure 6). Examples from literature are protamine competing with the marker ion $[Ru(NH_3)]^{3+}$ or protamine/heparin competing with $[Fe(CN)_6]^{3-}$ on a thioctic acid layer[1] and specific complexation of metal ions[46] competing with $[Ru(NH_3)_6]^{3+}$. To reach sensitivity (suppression of the current of an electrocatalytic marker ion) high affinity constants are required between analyte and sensing layer.

(b) Neutral analytes. Neutral analytes have been successfully measured with the ICS system, e.g. the detection of estrogen with its binding protein immobilized on an electrode[11] and aryl hydrocarbons on the corresponding receptor-modified electrodes[12] using $[Fe(CN)_6]^{4-/3-}$. It is explained by the loss of surface charge on the sensing layer due to complexation of the analyte, and as expected, the reported sensors all show a decrease of the marker ion current (type b2) upon analyte addition. Closing the interstitial pores with a long-chain thioalkane in this work (eq 19) is related to these experiments.

(c) Analytes with a bioconjugated fixed charge. If the analyte is a peptide or protein, the peripheral charges of analyte and sensing layer depend on the solution pH, and the ICS is difficult to optimize (association constant, best pH range for marker ion current change). A fixed pH-independent charge can be introduced on protein analytes via bioconjugation. Cytochrome *c* in Figure 8 is used as sensing layer rather than analyte but shows this principle. It has lost its pH dependence after bioconjugation with **Vio-IV** (Figure 8).

(d) Analytes with electrocatalytic properties or with a bioconjugated electrocatalyst. This configuration is probably the one with the highest signal amplification potential. In Figure 8 electrocatalysis of the exergonic reduction of $[Fe(CN)_6]^{3-}$ by a protein-confined viologen (interpreted here as analyte) is observed much below that of monolayer coverage. A similar electrocatalytic situation has been reported for a DNA-modified electrode.[13]

Moreover, we consider the optimization of the pH range, the choice of the marker ion, the incorporation of persistent charges on the analyte (or analytes with bioconjugated electrocatalysts) as the most promising aspects in the further development of ion channel sensor systems.

Conclusions

The mechanism of charge propagation in "ion channel sensors" based on protein-modified electrodes and highly charged electroactive marker ions has been elucidated. The broad approach and the resemblance of the results with those obtained with SAM-modified electrodes demonstrates the generality of our findings.

Close to diffusion-controlled currents are observed at the modified electrodes if the charge of the marker ions is opposite from the prevailing charge of the domains on the protein. On the other hand, if marker ion and dominating protein domain charges have the same sign, essentially no current is observed. Neutral redox species of similar size exhibit almost diffusion-controlled currents independent of pH. The pores between adjacent proteins constitute a diffusion barrier for equally charged marker ions. As proteins exhibit a pH-adjustable surface

(43) Tong, Y. H.; Han, X. J.; Song, Y. H.; Jiang, J. G.; Wang, E. K. *Biophys. Chem.* **2003**, *105*, 1.
(44) Takehara, K.; Aihara, M.; Ueda, N. *Electroanalysis* **1994**, *6*, 1083.
(45) Takehara, K.; Aihara, M.; Miura, Y.; Tanaka, F. *Bioelectrochem. Bioenerg.* **1996**, *39*, 135.
(46) Ito, T. *J Electroanal. Chem.* **2001**, *495*, 87.

charge, there exists a sigmoidal transition from the conducting to the isolating situation as a function of pH.

A marker ion with at least two charges binds electrostatically to oppositely charged protein domains and then shows a current modulated by the analyte. Innocent, nonelectroactive ions can substitute marker ions on the protein. Thereby, the current is suppressed. The reason is that the charge propagation through the protein layer is based on electron shuttling by surface-confined marker ions.

The same mechanistic picture holds for the other type of gating, i.e., marker-ion current enhancement. The starting situation is nonconductive, e.g., a negatively charged marker ion in combination with negatively charged protein domains. The analyte, or gating ion, is a multicharged cation. It coordinates in the micromolar range to the domain and inverts the apparent surface charge, so that the marker ion can coordinate on top of the gating ion. This supramolecular assembly, consisting of charged domain−analyte ion−marker ion allows again for electron shuttling along surface-confined marker ions. The amplification factor in this situation is significant. (Sub-)micromolar analyte concentrations can gate currents in the 100 μA/cm^2 range.

For both cases the current is either collected by radial diffusion in the solution above the protein layer toward the pore entrances or by ET shuttling in extended, marker ion-loaded domains on the protein surface. Within the funnel, representing the bottleneck for the conduction, the dominating mechanism of charge propagation is definitely electron shuttling between adjacent marker ions. The funnel region translates, therefore, changes in surface charge most efficiently into changes in current.

This work describes mainly the mechanism of charge propagation of marker ions through protein layers, but the conclusions are of general validity for any polyelectrolyte-type sensing layer consisting of macromolecules with a surface charge dictated by the pH. Moreover, our results are also of interest with respect to the optimization of real ICS systems applied to bioanalytical problems.

Acknowledgment. P.S. thanks Prof. S. Speller for the use of AFM facilities and the SFB 431 for financial support. T.H.D. thanks the Federal State of Niedersachsen for the fellowship granted through the International Graduate School of Science at the University of Osnabrück.

Supporting Information Available: Experimental details for the synthesis of the viologen-type marker ions, the viologen label and its protein conjugate, and *N*-(2-mercaptoethyl)-ferrocene carboxamide (**TF**); QCM, AFM, and EQCM measurements; pH−DPV titration curve for **Vio-II** at Tg−Au; model for protein layer with interstitial void; CV of $[Fe(CN)_6]^{4-}$ on Tg−Au before and after treatment with dodecane thiol; and CV of **TF** SAMs-modified Au electrode in the absence and presence of $[Fe(CN)_6]^{4-}$. This material is available free of charge via the Internet at http://pubs.acs.org.

JA051574C